Geol. Mag. **145** (*4*), *2008, pp. 475–489. © 2008 Cambridge University Press*
doi:10.1017/S0016756808004561 *Printed in the United Kingdom*

Middle Neoproterozoic syn-rifting volcanic rocks in Guangfeng, South China: petrogenesis and tectonic significance

WU-XIAN LI*, XIAN-HUA LI*† & ZHENG-XIANG LI‡

*Key Laboratory of Isotope Geochronology and Geochemistry, Guangzhou Institute of Geochemistry, Chinese Academy of Sciences, Guangzhou 510640, China
†State Key Laboratory of Lithospheric Evolution, Institute of Geology and Geophysics, Chinese Academy of Sciences, Beijing 100029, China
‡Institute of Geoscience Research, Department of Applied Geology, Curtin University of Technology, GPO Box U1987, Perth, WA 6845, Australia

(*Received* 22 May 2007; *accepted* 23 July 2007; First published online 8 April 2008)

Abstract – Middle Neoproterozoic igneous rocks are widespread in South China, but their petrogenesis and tectonic implications are still highly controversial. The Guangfeng middle Neoproterozoic volcani-sedimentary succession was developed on a rare Sibaoan metamorphic basement (the Tianli Schists) in the southeastern Yangtze Block, South China. This paper reports geochronological, geochemical and Nd isotopic data for the volcanic rocks in this succession. The volcanic rocks consist of alkaline basalts, andesites and peraluminous rhyolites. SHRIMP U–Pb zircon age determinations indicate that they were erupted at 827 ± 14 Ma, coeval with a widespread episode of anorogenic magmatism in South China. Despite showing Nb–Ta depletion relative to La and Th, the alkaline basalts are characterized by highly positive εNd(T) values (+3.1 to +6.0), relatively high TiO_2 and Nb contents and high Zr/Y and super-chondritic Nb/Ta ratios, suggesting their derivation from a slab melt-metasomatized subcontinental lithospheric mantle source in an intracontinental rifting setting. The andesites have significantly negative εNd(T) values (−9.3 to −11.1) and a wide range of SiO_2 contents (57.6–65.6 %). They were likely generated by the mixing of fractionated basaltic melts with felsic melts derived from the Archaean metasedimentary rocks in the middle to lower crust. The rhyolites are highly siliceous and peraluminous. They are characterized by depletion in Nb, Ta, Sr, P and Ti and relatively high εNd(T) values (−3.0 to −4.8), broadly similar to those of the adjacent *c.* 820 Ma peraluminous granitoids derived from the Mesoproterozoic to earliest Neoproterozoic sedimentary source at relatively shallow levels. We conclude that the Guangfeng volcanic suite is a magmatic response of variant levels of continental lithosphere (including lithospheric mantle and the lower-middle to upper crust) to the middle Neoproterozoic intracontinental rifting possibly caused by mantle plume activity.

Keywords: Neoproterozoic, geochemistry, volcanic rocks, rift basin, South China.

1. Introduction

Middle Neoproterozoic igneous rocks are widespread in South China (Fig. 1a), but their petrogenesis and tectonic implications are still hotly debated (e.g. Li *et al.* 1999, 2002*a*, 2003*a*,*b*, 2006; Li, Li & Li, 2005; Zhou *et al.* 2002*b*,*c*, 2006*a*,*b*; Wang *et al.* 2004, 2006). Based on similarities between the *c.* 820 Ma mafic dykes and sills in South China and the coeval, plume-related Gairdner Dyke Swarm in Australia (Zhao, Malcolm & Korsch, 1994; Wingate *et al.* 1998), and the presence of same-aged granitic intrusions (Li, 1999) accompanied by continental-scale doming and unroofing, Li *et al.* (1999) proposed that a *c.* 825 Ma mantle plume beneath South China triggered the continental rifting and eventually led to the breakup of Rodinia. Recently, these authors further demonstrated that two episodes of widespread bimodal magmatism occurred at *c.* 830–795 Ma and *c.* 780–745 Ma, respectively, in South China; these age patterns are similar to those of middle Neoproterozoic bimodal magmatism in numerous other Rodinian continental blocks such as Australia, India, Madagascar, Seychelles, southern Africa and Laurentia (Li *et al.* 2003*b* and references therein). Such globally widespread magmatism requires a large and sustained heat source, which Li *et al.* (2003*b*) suggested as reflecting the presence of a mantle superplume beneath Rodinia that led to the break-up of the supercontinent in the Neoproterozoic. In addition, these workers also argued that the Yangtze and Cathaysia blocks amalgamated to form the coherent South China Block during the Sibao orogenesis at *c.* 1.1–0.9 Ga (e.g. Li *et al.* 2002*b*, 2006, 2007*c*; Greentree *et al.* 2006; Li & Li, 2003; Ye *et al.* 2007), thus precluding the occurrence of any 860–740 Ma magmatic arc in the interior of the South China Block.

Zhou and co-workers (e.g. Zhou *et al.* 2002*b*, *c*, 2006*a*,*b*), on the other hand, interpreted the 860–760 Ma magmatic rocks as products of subduction around the Yangtze Block, a part of the South China

†Author for corresponence: lixh@gig.ac.cn

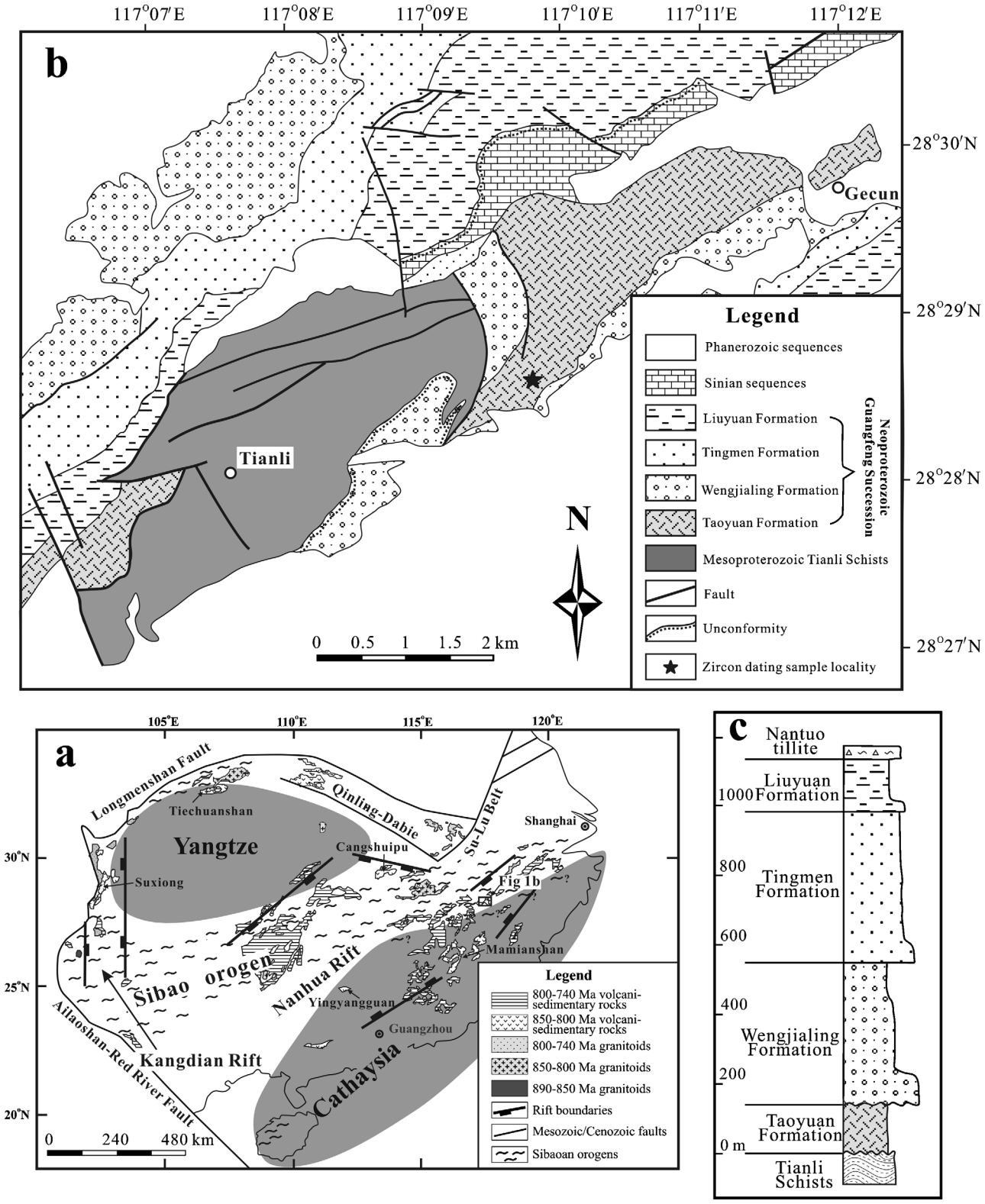

Figure 1. (a) Neoproterozoic rift basin, Sibaoan Orogen and distribution of magmatic rocks in South China (modified after Li *et al.* 2002*b*, 2003*b*; Wang & Li, 2003), (b) Geological map of the Guangfeng region (modified after the 1:50 000 geological map), and (c) Neoproterozoic stratigraphic column of Guangfeng region (after Li *et al.* 2003*c*).

Block. In their model, the South China Block was either an isolated continent, or was located on the periphery of Rodinia during Neoproterozoic times. Others interpreted some of the *c.* 820–800 Ma granitic rocks as products related to the continental collision between the Yangtze and Cathaysia blocks or post-collisional extensional collapse (e.g. Wang *et al.* 2006; Wu *et al.* 2006), rather than the products of crustal

anatexis caused by conductive heating above a mantle plume (Li *et al.* 2003*a*).

The Neoproterozoic Guangfeng succession is located in the northern margin of the Northern Zhejiang sub-basin, part of the broader Nanhua basin (Fig. 1b) (Wang & Li, 2003). The outcrop is a small (about 300 km^2) but well-preserved Neoproterozoic volcanisedimentary succession (Wang & Gao, 2003). Volcanic rocks occur at the bottom of the basin that overlies on the Mesoproterozoic Tianli Schists (Li *et al.* 2007*c*) with a high-angle unconformity. Therefore, they were formed after the Sibaoan orogenesis. In this paper we report new SHRIMP U–Pb zircon ages and geochemical and Nd isotopic results of the volcanic rocks from the Guangfeng succession, with the aim of characterizing their petrogenesis and tectonic implications.

2. Geological setting and petrography

The South China Block is bounded by the Qinling–Dabie–Sulu orogenic belt to the north, the Longmenshan Fault to the northwest, and the Ailaoshan–Red River Fault to the southwest (Fig. 1a). It is generally believed to have been formed through amalgamation of the Yangtze and Cathaysia blocks. The oldest rocks in the Yangtze Block are the 3.2 to 2.9 Ga Kongling complex (e.g. Qiu *et al.* 2000; Zhang *et al.* 2006*a*) occurring near the Yangtze Gorge. More recently, Zheng *et al.* (2006) and Zhang *et al.* (2006*b*) suggested that the Archaean to Palaeoproterozoic basement is probably widespread beneath the Yangtze Block. The oldest igneous rocks found in the Cathaysia Block are the *c.* 1.8 Ga granite and metavolcanic rocks (e.g. Li, 1997; Li & Li, 2007).

Neoproterozoic igneous rocks are widespread in South China, with most occurring in the Kangdian Rift (a SN-trending failed rift along the western Yangtze Block) and the Nanhua Rift (a broad, NE-trending rift basin between the southern Yangtze and northern Cathaysia blocks, Fig. 1a). They were floored unconformably by strongly deformed, late Mesoproterozoic to early Neoproterozoic successions and *c.* 825–820 Ma granitoids that were exposed to the surface soon after emplacement due to rapid continental-scale doming and unroofing (Li, *et al.* 1999, 2003*a*,*b*; Wang & Li, 2003). The Nanhua Rift can be further subdivided into three sub-rift basins, namely the Hunan–Guangxi sub-basin, the Jiangnan Ridge sub-basin and the Northern Zhejiang sub-basin (Wang & Li, 2003). The Guangfeng succession is located at the northern margin of the Northern Zhejiang sub-basin along the southeastern margin of the Yangtze Block (Fig. 1a, b).

The Guangfeng succession consists of a basal conglomerate unit and volcanic rocks, and lacustrine, fluvial and littoral marine facies sedimentary rocks (Wang & Gao, 2003; Li *et al.* 2003*c*). It is subdivided into four formations according to the petrological assemblages and sedimentological characteristics (Fig. 1c). They are, from bottom to top: (1) the Taoyuan Formation, consisting predominantly of volcanic and pyroclastic rocks that uncomfortably overlie the Mesoproterozoic Tianli Schists, (2) the Wenjialing Formation, comprising volcanic conglomerate overlying both the Tianli Schists and the Taoyuan Formation volcanic rocks, (3) the Tingmeng Formation, consisting of purplish-red, thick-bedded to massive fluvial feldspathic litharenite, quartz feldspathic litharenite, siltstone and silty mudstone, and (4) the Liuyuan Formation, comprising thick-bedded pebbly quartz-sandstone with well-developed littoral marine cross-beddings. Overlying the Liuyuan Formation is the Nantuo glacial-marine deposits (tillite), which is a Marinoan-aged glaciation event dated at *c.* 600–630 Ma (Zhou *et al.* 2004). Two unpublished U–Pb ages of *c*. 820 Ma have previously been quoted for the andesite and rhyolite in the Taoyuan Formation (Zhang, Yan & Yan, 1991; Wang & Gao, 2003).

Volcanic rocks in the Taoyuan Formation include basaltic and andesitic rocks at the bottom of the formation, and felsic rocks mainly at the top of the formation, with an estimation of the basalt:andesite:rhyolite ratios being roughly 4:1:5 (Guan & Yu, 1993). The basaltic rocks include porphyritic olivine basalts, which are dark-green in colour, containing sparse plagioclase and olivine phenocrysts, 0.7–1.5 mm in size. The olivine and plagioclase phenocrysts were altered to serpentine and carbonate, respectively. The groundmass of the basaltic rocks is aphanitic to microlitic (0.05–0.08 mm), consisting of oligoclase/andesine, olivine, augite(?) and Fe–Ti oxide with strong carbonation and chloritization alteration. The andesitic rocks are brick-red in colour, containing abundant (30–50 %) plagioclase and minor amounts of K-feldspar(?) and pyroxene(?) phenocrysts with variable grain sizes between 0.2 mm and 3 mm. All phenocryst minerals were strongly altered. The groundmass of the andesitic rocks is microlitic, composed predominantly of plagioclase and sparse Fe–Ti oxides, with most minerals being altered (carbonation and chlorization). The felsic rocks are light-grey in colour, containing sparse quartz, plagioclase and K-feldspar phenocrysts. The groundmass of the felsic rocks is aphitic to microlitic with weakly rhyotaxitic structure, consisting of quartz, plagioclase and K-feldspar, and with variable degrees of sericitization.

3. Analytical methods

Zircons were separated using standard density and magnetic separation techniques. Zircon grains, together with zircon U–Pb standard TEMORA, were cast in an epoxy mount, which was then polished to section the crystals in half for analysis. Zircons were documented with transmitted and reflected light micrographs and cathodoluminescence (CL) images as a guide to

Table 1. SHRIMP U–Pb zircon data for Guangfeng rhyolite

Spot	U (ppm)	Th (ppm)	$^{232}Th/^{238}U$	f_{206}%	$^{206}Pb^*/^{238}U$ (±1σ)		$^{207}Pb*/^{235}U$ (±1σ)		$^{207}Pb*/^{206}Pb*$ (±1σ)		$^{206}Pb*/^{238}U$ age (Ma) (±1σ)	
1.1	369	240	0.67	0.98	0.1333	0.0029	1.366	0.095	0.0743	0.0051	806.7	17
2.1	174	133	0.79	0.55	0.1406	0.0034	1.286	0.054	0.0663	0.0026	848.2	19
3.1	417	394	0.98	1.72	0.1412	0.0028	1.320	0.091	0.0678	0.0046	851.7	16
4.1	338	168	0.51	1.88	0.1387	0.0029	1.243	0.075	0.0650	0.0038	837.2	17
5.1	464	353	0.79	2.38	0.1335	0.0026	1.213	0.070	0.0659	0.0037	807.7	15
6.1	561	425	0.78	3.25	0.1361	0.0026	1.293	0.079	0.0689	0.0041	822.4	15
7.1	807	431	0.55	3.65	0.0776	0.0015	0.801	0.049	0.0749	0.0045	481.7	9
8.1	201	118	0.61	1.96	0.1392	0.0034	1.537	0.086	0.0801	0.0043	840.0	19
9.1	229	146	0.66	0.26	0.1421	0.0032	1.322	0.043	0.0675	0.0020	856.4	18
10.1	746	669	0.93	4.48	0.1301	0.0027	1.317	0.152	0.0734	0.0084	788.4	16
11.1	389	268	0.71	1.59	0.1348	0.0038	1.312	0.067	0.0706	0.0034	815.3	22
12.1	239	136	0.59	0.38	0.1432	0.0046	1.333	0.072	0.0675	0.0034	862.9	26
13.1	302	239	0.82	1.18	0.1302	0.0040	1.271	0.067	0.0708	0.0035	789.2	23
14.1	244	158	0.67	0.35	0.1443	0.0045	1.328	0.062	0.0667	0.0028	869.1	25
15.1	483	555	1.19	6.43	0.1229	0.0036	1.354	0.129	0.0799	0.0074	747.0	21
16.1	542	432	0.82	1.77	0.1375	0.0037	1.417	0.064	0.0747	0.0031	830.5	21

Data in this table were calculated after ^{204}Pb corrections. The common Pb compositions were estimated from ^{204}Pb counting, assuming an isotopic composition of Broken Hill lead related to surface contamination (Nelson, 1997). All errors are 1 sigma (1σ).

isotopic analytical spot selection and the mount was vacuum-coated with high-purity gold. U–Pb isotopic compositions were analysed by using the SHRIMP II ion microprobe at the Beijing SHRIMP Center, Chinese Academy of Geological Sciences. U–Th–Pb ratios were determined relative to the TEMORA standard zircon with $^{206}Pb/^{238}U = 0.0668$ corresponding to 417 Ma (Black *et al.* 2003), and the absolute abundances were calibrated to the standard zircon SL13. Analyses of the TEMORA standard zircon were interspersed with those of unknown grains, following operating and data processing procedures similar to those described by Williams (1998). Measured compositions were corrected for common Pb using the ^{204}Pb-method, and an average crustal composition (Cumming & Richards, 1975) appropriate to the age of the mineral was assumed. Uncertainties on individual analyses are reported at the 1σ level, and mean ages for pooled $^{206}Pb/^{238}U$ results are quoted at the 95 % confidence level. U–Pb zircon data are listed in Table 1.

Because the basaltic and andesitic rocks are variably carbonatized, the rock powders were washed using dilute acetic acid to minimize the alteration effect before analyses. Major element oxides and trace elements were determined using a Rigaku ZSK100e XRF on fused glass beads and a Perkin-Elmer Sciex ELAN 6000 ICP-MS, respectively, at the Guangzhou Institute of Geochemistry, Chinese Academy of Sciences. Analytical procedures were similar to those described by Li *et al.* (2000, 2005). A mixture of 0.5 g powdered samples and 4 g $Li_2B_4O_7$ was fused as a glass bead for XRF analysis. A loss-on-ignition (LOI) measurement was undertaken on samples of dried rock powder by heating in a pre-ignition silica crucible to 1000 °C for one hour and recording the percentage weight loss. Analytical uncertainties of major elements are between 1 % and 5 %. About 50 milligrams of each powdered sample were dissolved in a high-pressure Teflon bomb for 24 hours using a HF+HNO_3 mixture to ensure complete sample digestion. Rh was used as an internal standard to monitor signal drift during counting. The USGS standards BCR-1, BHVO-1, W-2, G-2 and GSP-1 were used for calibrating element concentrations of measured samples. Analytical precision is generally better than 3 % for most trace elements.

The Nd fraction was separated by passing through cation columns followed by HDEHP columns. Nd isotopic compositions were determined using a Micromass Isoprobe multi-collector ICP-MS (MC-ICP-MS) at the Guangzhou Institute of Geochemistry. Analytical procedures were similar to those described by Li *et al.* (2004). Samples were taken up in 2 % HNO_3, and the aqueous solutions were introduced into the MC-ICPMS using a Meinhard glass nebulizer with an uptake rate of 0.1 ml/minute. The inlet system was washed out for five minutes between analyses using high-purity 5 % HNO_3, followed by a blank solution of 2 % HNO_3, from which the sample solutions were prepared. The Isoprobe MC-ICPMS was operated in a static mode, and yielded $^{143}Nd/^{144}Nd = 0.512125 \pm 11$ (2σ) on 14 runs for the Shin Etsu JNdi-1 standard during this study. Measured $^{143}Nd/^{144}Nd$ ratios were normalized to $^{146}Nd/^{144}Nd = 0.7219$. The reported $^{143}Nd/^{144}Nd$ ratios are adjusted relative to the Shin Etsu JNdi-1 standard of 0.512115, corresponding to the La Jolla standard of 0.511860 (Tanaka *et al.* 2000).

4. Results

4.a. SHRIMP U–Pb zircon age

Sample 06GDB15-1 (28°28′35″ N; 117°09′50″ E) is a rhyolite collected from the top of the Taoyuan Formation at the Shilong Reservoir. Zircon grains from

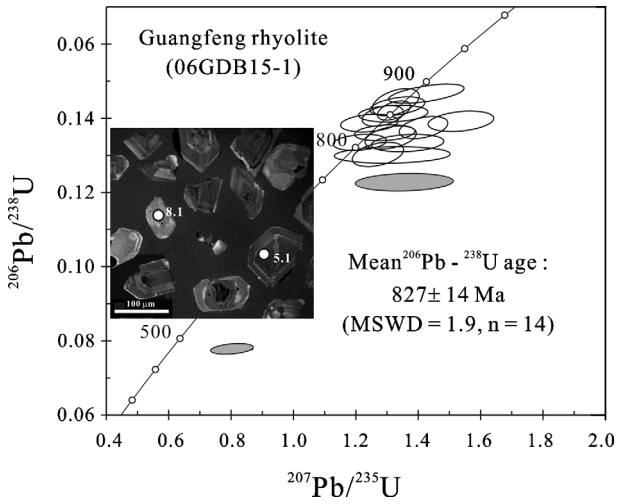

Figure 2. U–Pb zircon concordia diagram for the Guangfeng rhyolite. Inset shows representative zircon CL images. Data not included in the calculated age for the sample are shown as grey-filled symbols.

this sample are mostly euhedral, ranging from 50 to 100 μm in length, with length to width ratios of 1:1 to 2:1. They are relatively transparent and colourless, although a few are dark brown and turbid. Euhedral concentric zoning is common in most zircons under CL images and no inherited zircon cores were visible (Fig. 2 inset). Sixteen analyses of 16 zircons were obtained in sets of five scans during a single session (Table 1). They have highly variable abundance of U (174–807 ppm) and Th (118–669 ppm). Th/U ratios vary between 0.51 and 1.19, mostly clustering around 0.5–0.8. Common Pb varies, with f_{206} values falling in the range of 0.26 % to 6.43 %. Apart from two analyses (spots 7.1 and 15.1) that are obviously discordant due to partial loss of radiogenic Pb (Fig. 2), the remaining 14 analyses gave $^{206}Pb/^{238}U$ ratios indistinguishable within analytical errors, and their weighted mean yields an age of 827 ± 14 Ma (95 % confidence interval). This age is interpreted as the best estimate of the formation age of sample 06GDB15-1.

4.b. Major and trace element geochemistry

Twenty Guangfeng volcanic rock samples were used for major and trace elements analyses. The results are listed in Table 2. Because all samples underwent varying degrees of alteration which might have modified the contents of mobile components (Romer, Forster & Breitkreuz, 2001), the mobility of the major and trace elements needs to be evaluated. In general, zirconium, which is considered to be immobile during low-grade alteration of mafic to intermediate igneous rocks (Gibson *et al.* 1982), has been plotted against some major and trace elements (Fig. 3). Although the basalts have highest LOI (loss of ignition) values of between 4.85 % and 6.74 %, the high field-strength elements (HFSE: Nb, Ti, P, Th, Y and V) and rare earth elements (REE) show fairly homogeneous geochemical compositions, indicating that these elements are generally immobile, whereas some large ion lithophile elements (LILE: Sr) are mobile, as demonstrated by their obvious variations (Fig. 3). Similarly, the HFSE (Ti, P, Nb and Th) and REE show close correlations with Zr for the andesitic and rhyolitic samples, implying that they are generally immobile. On the contrary, the LILE (Sr, Rb) and V are scattered, suggesting that they are probably mobile during alteration. Therefore, mainly the immobile elements, such as HFSE (Ti, P, Nb, Ta, Zr, Hf, Th, V) and REE, are used for further petrogenetic discussions.

The basaltic rocks are characteristically high in TiO_2 (2.07–2.16 %), P_2O_5 (1.02–1.05 %), Al_2O_3 (17.12–17.67 %) and Nb/Y ratio of 0.86–0.92, uniform in SiO_2 (51–53.4 %) and low in MgO (2.2–3.5 %), belonging to alkaline basalts. The andesitic rocks, on the other hand, have considerably higher and variable SiO_2 (57.6–65.6 %), but lower MgO (0.49–0.70 %) and TiO_2 (0.84–1.21 %), except for sample 03SC05-2 which has relatively high MgO (2.64 %). The rhyolitic rocks are highly siliceous ($SiO_2 = 74.3$–76.6 %) and peraluminous (A/CNK > 1.6). The three groups of volcanic rocks have different evolved trends in most Zr versus major and trace elements plots (Fig. 3, Table 2), especially in Zr v. TiO_2, P_2O_5, Th and Nb plots, suggesting that they are not cogenetic.

On the chondrite-normalized diagrams (Sun & McDonough, 1989), all basaltic rocks have uniform and significant LREE-enriched patterns (Fig. 4a) with $La_N/Yb_N = 17.6$–21.2, and slightly positive Eu anomalies ($\delta Eu = 1.1$–1.2). Contrarily, the andesitic rocks have variable REE abundances and LREE-enriched patterns (Fig. 4b) with moderate Eu negative anomalies ($\delta Eu = 0.7$–0.9). They are characterized by steeply right-inclined LREE patterns ($La_N/Sm_N = 4.4$–5.8) but gently right-inclined HREE patterns ($Gd_N/Yb_N = 1.5$–2.2). The rhyolitic rocks show uniform LREE-enriched and MREE to HREE-flat patterns, with $La_N/Sm_N = 5.1$–6.0, $Gd_N/Yb_N \approx 1.0$ and significant Eu negative anomalies ($\delta Eu = 0.50$–0.55) (Fig. 4c). It is noted that their REE patterns are strikingly similar to those of the regional *c.* 820 Ma peraluminous granitoids from southern Anhui and northern Jiangxi provinces (Li *et al.* 2003*a*; Wu *et al.* 2006).

On the primitive mantle-normalized trace element diagrams (Fig. 4d), the basaltic rocks show 'humped' patterns characterized by variable enrichments in most incompatible trace elements but depletions in Nb and Ta relative to neighbouring elements, resembling those of the Cenozoic extension-related basalts in the Basin and Range Province (e.g. Hawkesworth *et al.* 1995). The andesitic rocks are characterized by obvious Nb and Ta depletions relative to La and Th, with Nb/La = 0.24–0.36 and Nb/Th = 0.87–1.01. Their primitive mantle-normalized trace element patterns resemble that of the average middle crust (Fig. 4e). The rhyolitic rocks have

Table 2 Major and trace elements results for Guangfeng volcanic rocks

Rock type	03SC05–4 B	03SC05–5 B	03SC05–6 B	03SC05–7 B	03SC05–8 B	03SC05–9 B	03SC05–10 B	03SC05–1 A	03SC05–2 A	03SC05–3 A	03SC06–1 A	03SC06–2 A	03SC06–3 A	03SC06–4 A	02SC09–4 A	02SC10–1 A	03SC04-1 RH	03SC04-2 RH	03SC04-3 RH	03SC04-4 RH
Major oxides (%)																				
SiO_2	51.31	51.61	51.79	52.85	50.99	52.05	53.38	57.62	57.85	62.74	63.17	59.46	62.91	59.57	65.60	61.32	75.18	75.44	74.29	76.63
TiO_2	2.13	2.07	2.13	2.13	2.09	2.09	2.16	0.94	0.99	0.98	0.94	1.21	1.11	1.14	0.84	0.98	0.22	0.21	0.23	0.20
Al_2O_3	17.67	17.17	17.42	17.42	17.26	17.12	17.57	19.35	19.01	17.90	16.84	17.64	17.51	20.12	17.18	18.72	13.50	13.54	14.97	12.60
Fe_2O_3	8.99	10.00	9.61	9.65	9.99	9.75	8.97	8.94	7.13	7.30	8.62	11.11	8.46	7.88	4.23	7.74	1.72	1.63	1.86	1.82
MnO	0.07	0.06	0.06	0.04	0.08	0.07	0.04	0.02	0.10	0.03	0.06	0.06	0.03	0.02	0.07	0.03	0.04	0.06	0.03	0.04
MgO	2.16	3.46	3.10	3.63	2.75	2.80	3.18	0.49	2.64	0.52	0.51	0.70	0.54	0.54	0.68	0.62	0.48	0.46	0.55	0.43
CaO	4.59	4.95	5.18	3.78	5.51	4.49	4.24	0.73	1.27	0.87	0.51	0.48	0.51	0.59	0.84	0.51	0.44	0.24	0.15	0.50
Na_2O	2.74	2.63	2.61	2.53	2.83	2.66	2.67	6.03	5.96	5.32	4.25	2.02	3.18	3.50	4.63	3.69	1.85	2.88	0.17	2.47
K_2O	2.75	2.32	2.25	2.56	2.44	2.51	2.56	2.78	1.70	2.45	2.50	3.89	3.25	3.80	2.32	3.47	3.81	3.41	4.73	2.92
P_2O_5	1.03	1.03	1.05	1.02	1.05	1.02	1.03	0.34	0.30	0.38	0.23	0.28	0.25	0.27	0.27	0.34	0.04	0.03	0.02	0.03
LOI	6.74	5.04	4.90	4.85	5.45	5.66	4.89	1.79	3.05	2.03	2.21	2.93	2.61	3.01	4.03	2.74	2.48	2.19	2.69	2.14
Total	100.18	100.34	100.09	100.46	100.44	100.20	100.68	99.04	100.01	100.52	99.84	99.76	100.36	100.45	100.70	100.13	99.77	100.09	99.69	99.79
Trace elements (ppm)																				
Sc	12.20	8.89	7.66	12.57	10.46	8.54	9.44	9.33	8.89	10.53	10.07	11.36	10.80	8.72	12.46	12.38	8.18	6.95	5.08	5.76
V	193	193	196	186	182	169	179	179	176	163	100	146	167	162	108	150	6.75	1.22	5.31	4.60
Co	21.2	26.2	23.8	25.3	23.9	22.4	24.7	11.7	27.9	16.9	15.6	18.5	13.0	17.6	10.6	14.0	1.84	0.86	1.76	1.58
Ni	22.7	26.9	26.4	28.0	26.5	25.2	36.2	20.3	34.2	24.9	15.2	34.7	25.4	18.3	40.5	25.4	19.32	2.75	3.75	3.33
Ga	18.2	18.5	18.8	19.0	18.2	17.3	18.3	19.8	20.1	19.8	14.8	19.9	18.1	20.0	16.2	22.3	16.2	9.64	18.1	12.6
Ge	0.96	0.98	0.99	1.06	1.02	0.96	1.00	0.85	0.83	0.94	0.92	1.00	1.06	1.03	1.07	1.40	1.34	0.82	1.09	1.22
Rb	37.4	33.1	30.7	39.2	32.3	33.6	35.8	116	61.4	114	82.9	133	116	140	57.8	149	144	76.8	174	104
Sr	738	847	884	625	898	748	718	229	382	314	92.0	62.6	101	103	135	267	63.9	39.2	40.0	58.1
Y	19.4	17.4	18.3	17.8	17.6	17.7	17.7	25.4	23.1	29.4	19.6	23.6	22.8	22.9	20.4	30.9	32.6	20.6	33.9	26.7
Zr	203	206	204	207	198	197	207	280	229	323	171	214	192	206	223	353	218	148	217	197
Nb	17.7	16.3	15.8	16.1	15.6	15.6	16.2	17.4	14.1	20.4	9.88	12.6	11.5	12.1	12.0	20.4	18.4	11.9	18.4	16.5
Ba	1100	1078	1078	1036	1068	1059	1066	404	461	443	252	447	356	391	583	442	274	251	231	228
La	42.6	44.1	41.4	43.5	40.7	37.6	42.7	65.5	44.2	60.4	35.2	37.6	44.5	33.8	44.7	86.2	54.5	31.6	41.9	43.7
Ce	89.1	92.3	86.9	92.4	85.6	76.4	88.7	112	86.1	117	70.2	69.8	87.7	66.2	85.0	152	105	50.5	85.1	67.6
Pr	11.6	11.9	11.3	12.1	11.1	10.1	11.7	13.4	9.62	12.9	8.12	8.40	10.2	7.90	9.22	17.9	9.90	5.57	7.24	7.79
Nd	44.6	46.9	44.5	46.7	42.9	39.6	45.7	45.6	34.2	45.1	29.8	31.3	37.7	29.1	34.1	64.0	33.0	18.7	25.4	25.7
Sm	7.75	7.84	7.53	7.82	7.34	6.72	7.67	7.33	5.60	7.39	5.08	5.50	6.33	5.41	5.41	9.57	6.01	3.42	5.32	4.68
Eu	2.39	2.46	2.46	2.40	2.38	2.24	2.43	1.59	1.26	1.51	1.33	1.28	1.47	1.37	1.06	1.97	0.97	0.54	0.84	0.74
Gd	5.85	5.84	5.41	5.82	5.44	5.46	5.61	5.38	4.76	5.86	4.03	4.77	4.71	5.02	4.73	8.00	4.88	3.23	4.79	4.15
Tb	0.81	0.78	0.73	0.79	0.73	0.73	0.76	0.83	0.72	0.95	0.62	0.72	0.71	0.75	0.73	1.21	0.82	0.55	0.89	0.72
Dy	4.18	3.79	3.84	4.09	3.72	3.62	3.94	4.66	4.06	5.47	3.54	4.23	4.22	4.26	4.05	6.11	5.17	3.37	5.58	4.51
Ho	0.75	0.67	0.68	0.68	0.66	0.67	0.67	0.90	0.82	1.04	0.74	0.84	0.84	0.83	0.81	1.22	1.12	0.68	1.10	0.92
Er	1.95	1.74	1.89	1.82	1.76	1.72	1.90	2.70	2.48	3.00	2.13	2.58	2.45	2.42	2.36	3.24	3.31	2.11	3.40	2.84
Tm	0.27	0.25	0.28	0.25	0.26	0.25	0.28	0.41	0.37	0.48	0.35	0.40	0.38	0.40	0.35	0.49	0.57	0.37	0.56	0.49
Yb	1.56	1.54	1.56	1.50	1.44	1.53	1.44	2.57	2.39	3.02	2.14	2.54	2.35	2.38	2.19	3.09	3.75	2.37	3.80	3.25
Lu	0.22	0.21	0.23	0.20	0.20	0.21	0.22	0.38	0.37	0.45	0.32	0.39	0.36	0.37	0.36	0.51	0.58	0.38	0.57	0.51
Hf	4.95	4.98	4.95	4.94	4.69	4.74	5.05	7.22	5.83	8.12	4.47	5.62	5.58	5.48	6.17	9.66	5.89	4.26	6.22	5.62
Ta	0.80	0.78	0.76	0.78	0.71	0.75	0.79	1.22	1.00	1.50	0.74	0.88	0.86	0.88	1.10	1.68	1.65	1.06	1.68	1.58
Pb	10.5	8.63	15.1	11.5	7.75	7.71	25.8	15.3	21.2	14.6	5.92	9.70	9.77	2.73	34.3	23.3	31.6	14.5	9.23	14.3
Th	2.49	2.50	2.54	2.55	2.46	2.40	2.64	19.1	15.4	23.03	9.75	12.7	11.9	12.2	15.5	27.0	24.0	15.7	24.9	21.6
U	0.49	0.48	0.48	0.51	0.47	0.46	0.51	4.90	3.87	5.94	1.88	2.17	2.53	3.28	4.27	5.44	4.62	2.85	4.97	4.16
T_{Zr} (°C)																	862	817		847

B – basalt; A – andesite; RH – rhyolite. Total iron as Fe_2O_3.
$T_{Zr} = 12\,900/(2.95 + 0.85M + \ln(496\,000/Zr_{melt}))$ (Miller, McDowell & Mapes, 2003), where M = (Na+K+2Ca)/(Al×Si) (Watson & Harrison, 1983).
T_{Zr} (°C) is not calculated for 03SC04-3 due to low M value of 0.5.

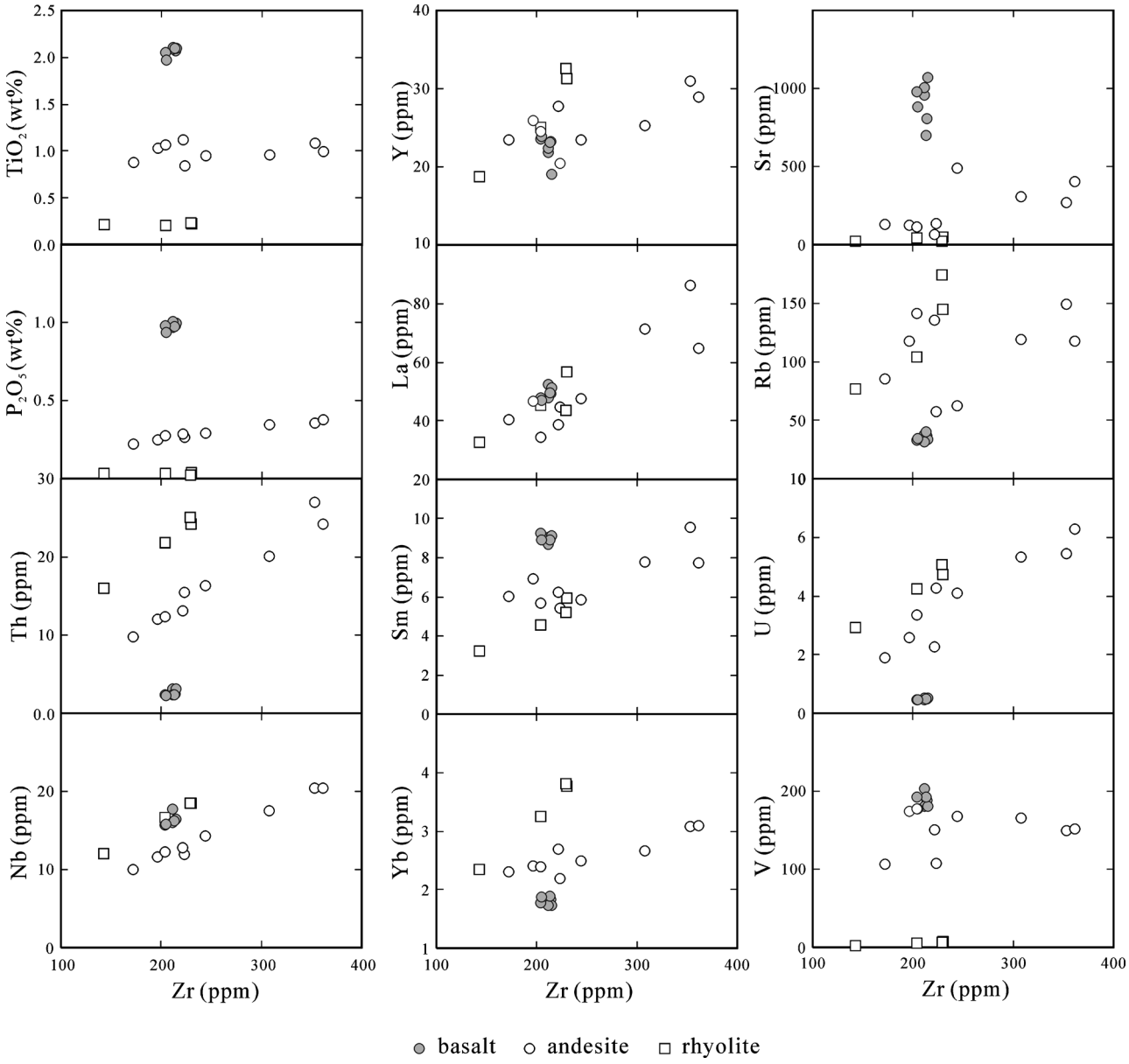

Figure 3. Plots of selected major and trace elements versus Zr.

strongly fractional patterns with significant depletions in Nb, Ta, Sr, P and Ti, due to fractional crystallization of plagioclase, apatite and Fe–Ti oxides, or as residual minerals in the source (Fig. 4f). Their patterns are similar to those of the average upper crust and the regional *c.* 820 Ma peraluminous granitoids (Li *et al.* 2003*a*; Wu *et al.* 2006).

4.c. Nd isotopes

Eleven samples were selected for Nd isotope analyses, including four basaltic rocks, four andesitic rocks and three felsic rocks. The results are listed in Table 3. The three groups of rocks have different Nd isotopic compositions. The basaltic samples have relatively constant $^{147}Sm/^{144}Nd$ (0.1013–0.1052) and $^{143}Nd/^{144}Nd$ (0.51229–0.51244) ratios, corresponding to initial $\varepsilon Nd(T)$ values of 3.1 to 6.0 and single-stage Nd model ages (T_{DM}) of 1.0–1.2 Ga. The andesitic rocks have significantly lower and uniform $^{147}Sm/^{144}Nd$ (0.0868–0.0991) and $^{143}Nd/^{144}Nd$ (0.51152–0.51158) ratios. Thus, they have significantly lower $\varepsilon Nd(T)$ values of -9.3 to -11.1 and older two-stage Nd model ages (T_{2DM}) of 2.3–2.4 Ga, suggesting a Palaeoproterozoic/Neoarchaean source for these rocks. The rhyolitic rocks show constant Sm–Nd isotopic compositions, with $^{147}Sm/^{144}Nd = 0.1103$–$0.1268$, $^{143}Nd/^{144}Nd = 0.51201$–$0.51202$, corresponding to $\varepsilon Nd(T)$ values of -2.9 to -4.7 and T_{2DM} ages of 1.7–1.9 Ga, in between those of the associated basaltic and andesitic rocks. The Sm–Nd isotopic compositions of the rhyolites are also comparable with those of the regional *c.* 820 Ma peraluminous granitoids (Li *et al.* 2003*a*; Wu *et al.* 2006).

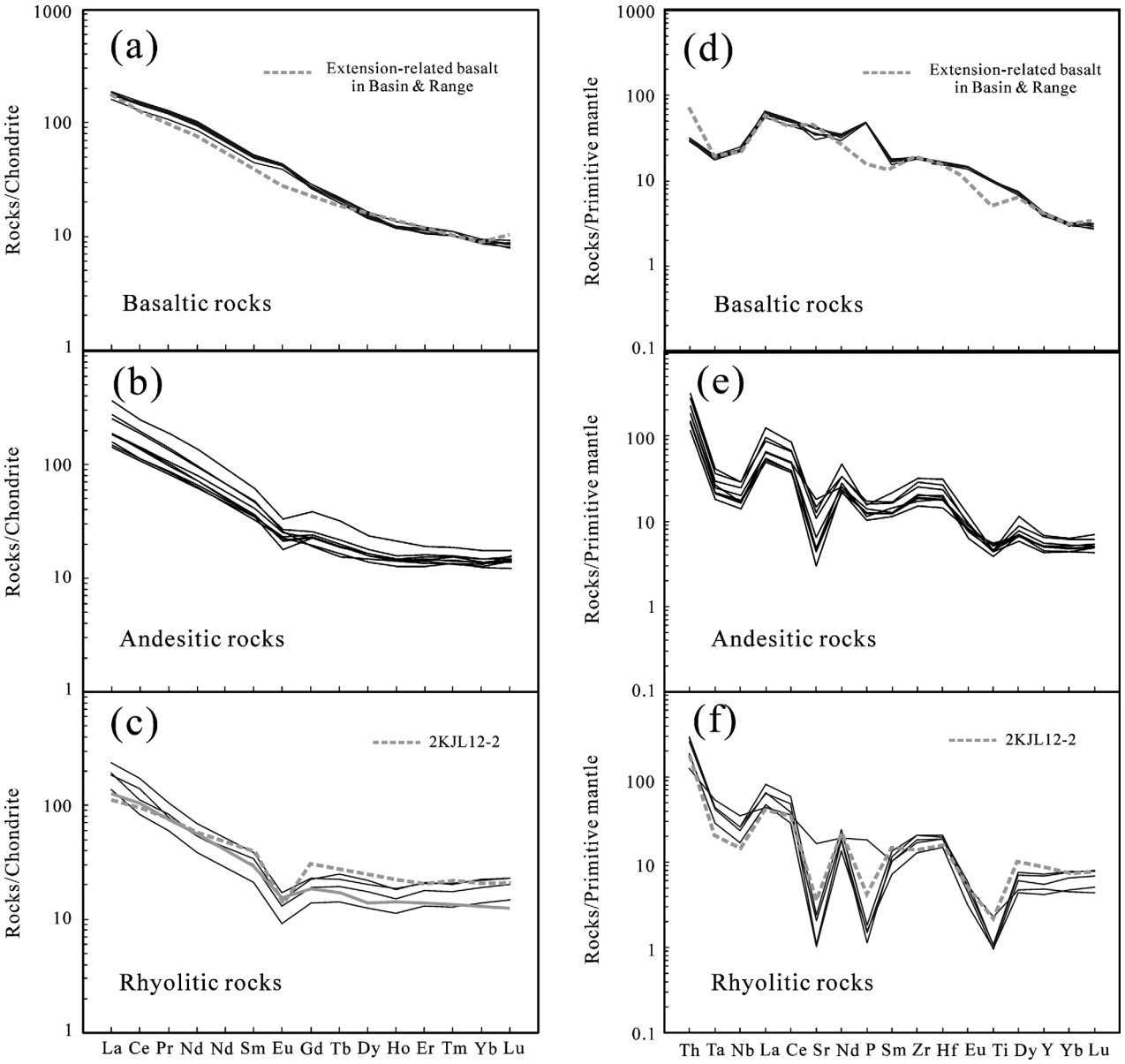

Figure 4. Chondrite-normalized REE diagrams (a–c) and primitive mantle-normalized trace elements diagrams (d–f). The basalts show REE and trace elements patterns similar to that of the Cenozoic extension-related basalts in the Basin & Range Province, and the rhyolites similar to that of the *c.* 825 Ma peraluminous granites. Data from Cenozoic basalts in the Basin & Range are after Hawkesworth *et al.* (1995). Sample 2KJL12–2 is a *c.* 820 Ma peraluminous granite in northern Jiangxi (after Li *et al.* 2003*a*). Normalization values are after Sun & McDonough (1989).

5. Petrogenesis

5.a. Basaltic rocks

The Guangfeng alkaline basaltic rocks are characterized by high HSFE contents such as Nb = 16–18 ppm, Zr = 197–207 ppm and TiO_2 = 2.07–2.16 %. On the tectonic discrimination diagrams of Ti–Zr–Y (Pearce & Cann, 1973) and Ti–Sm–V (Vermeesch, 2006), they plot exclusively into the OIB field, consistent with the same-aged Suxiong and Mamianshan alkaline basalts from the western Yangtze and northern Cathaysia blocks, respectively (Fig. 5a, b). In addition, the Guangfeng basalts are high in Zr/Y (11–12), exhibiting a broad geochemical similarity to the Cenozoic extension-related basalts in the Basin and Range Province (e.g. Hawkesworth *et al.* 1995).

The Guangfeng basalts show clear Nb–Ta negative anomalies (Nb/La = 0.37–0.41) (Fig. 4d), an often-quoted 'diagnostic' feature of arc basalts, but their geochemical characteristics are significantly different from those of arc basalts (Fig. 6). Depletion in Nb and Ta relative to La and Th in the intraplate basalts could be attributed to different processes including: (1) fractional crystallization of Ti-bearing minerals such as titanomagnetite, (2) contamination by crustal material during ascent of magmas, and (3) inheritance from

Table 3. Nd isotopic results for Guangfeng volcanic rocks

	Sm (ppm)	Nd (ppm)	$^{147}Sm/^{144}Nd$	$^{143}Nd/^{144}Nd$	$\pm 2\sigma_m$	εNd (T)	T_{DM} (Ga)	T_{2DM} (Ga)
Basalt								
03SC05-4	7.75	44.57	0.105	0.512366	0.000008	4.38	1.10	
03SC05-7	7.82	46.65	0.101	0.512328	0.000009	4.04	1.12	
03SC05-8	7.34	42.93	0.103	0.512292	0.000008	3.13	1.19	
03SC05-9	6.72	39.57	0.103	0.512287	0.000008	6.00	0.98	
Andesite								
03SC05-1	7.33	45.58	0.097	0.511528	0.000007	−11.14	2.12	2.39
03SC05-3	7.39	45.08	0.099	0.511548	0.000007	−10.96	2.13	2.38
02SC09-4	5.41	34.05	0.096	0.511577	0.000009	−10.05	2.03	2.31
02SC10-1	9.57	63.95	0.090	0.511584	0.000007	−9.34	1.93	2.25
Rhyolite								
03SC04-2	3.42	18.69	0.110	0.512024	0.000007	−2.86	1.66	1.72
03SC04-3	5.32	25.36	0.127	0.512017	0.000009	−4.72	1.98	1.87
03SC04-4	4.68	25.66	0.110	0.512009	0.000007	−3.14	1.68	1.75

T = 827 Ma, formation age of Guangfeng volcanic rocks. Single- and two-stage Nd model age, T_{DM} and T_{2DM} are calculated using formulas and parameters given by Li *et al.* (2003*a*).

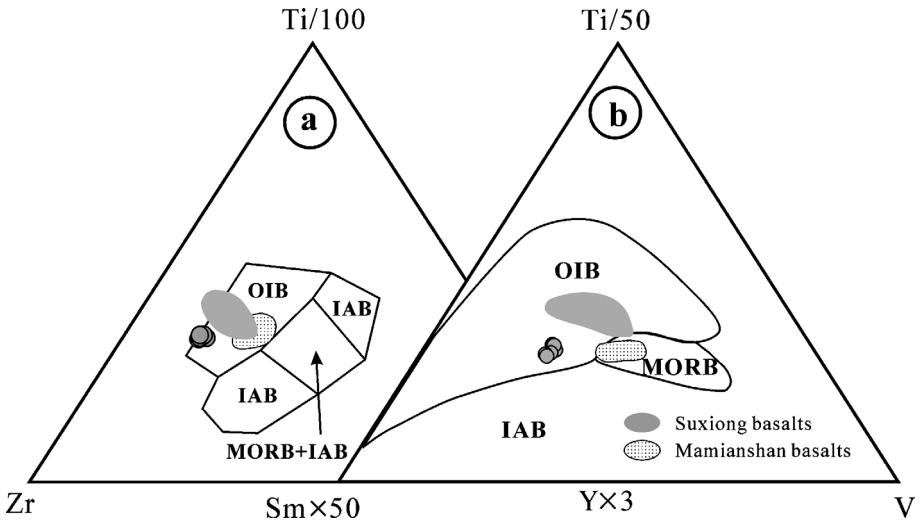

Figure 5. Tectonic discrimination diagram of (a) Ti–Zr–Y (Pearce & Cann, 1973) and (b) Ti–Sm–V (Vermeesch, 2006) for the Guangfeng basalts. The coveal Suxiong and Mamianshan basalts are shown for comparison (data after Li *et al.* 2002*a* and Li, Li & Li, 2005). Symbols are as in Figure 3.

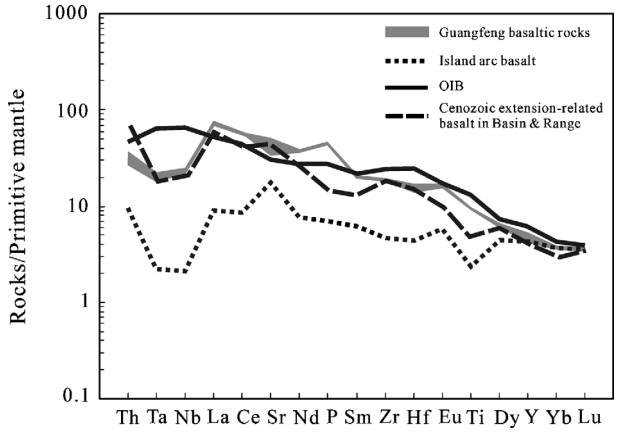

Figure 6. Comparison of incompatible trace element spider diagrams between the Guangfeng basalts and the average island-arc basalt (McCulloch & Gamble, 1991), OIB (Sun & McDonough, 1989) and Cenozoic basalt in the Basin and Range Province (Hawkesworth *et al.* 1995).

their mantle source which had been previously metasomatized by subduction-related fluids and/or melts. The Guangfeng basalts are characteristically high in TiO_2 (> 2.0 %) without visible Ti negative anomaly in the primitive mantle-normalized spidergrams (Fig. 4d), precluding significant fractional crystallization of titanomagnetite. It is noted that these basalts have lower Nb/La ratios (0.37–0.41) than those of crustal sources (Nb/La = 0.47–0.83: Rudnick & Fountain, 1995). Considering their high-positive $\varepsilon Nd(T)$ values, crustal contamination should have played very minor, if any, roles in the genesis of these basalts. Thus, their depletion in Nb–Ta relative to La and Th is most likely inherited from the mantle source that had been previously metasomatized by subduction-related fluids/melts. The Guangfeng basalts have super-chondritic Nb/Ta ratios of 20.5 to 22.1, inconsistent with same-aged Suxiong and Mamianshan basalts which have Nb/Ta ratios

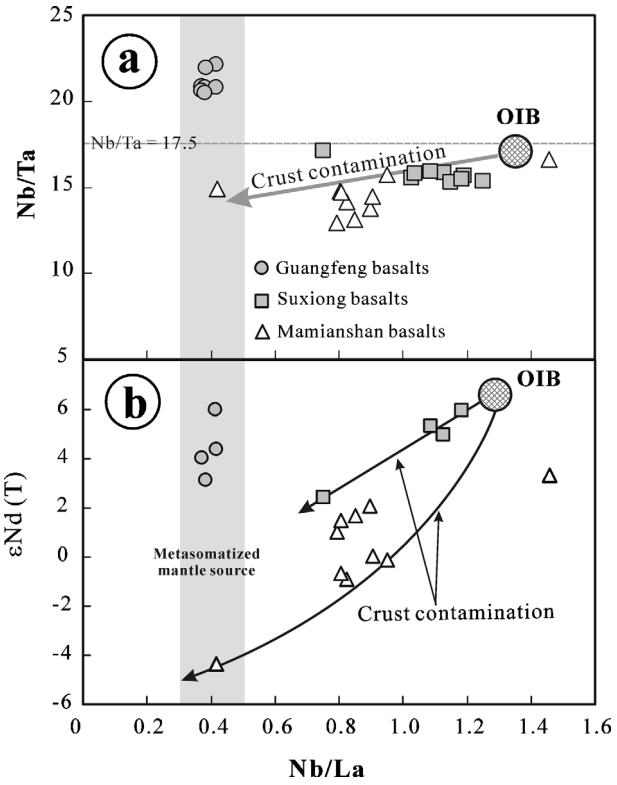

Figure 7. Plots of (a) Nb/La v. Nb/Ta and (b) Nb/La v. εNd(T) show that the Guangfeng basalts have super-chondritic Nb/Ta and low Nb/La ratios, suggesting derivation from siliceous melting of a metasomatized mantle source, whereas the same-aged Suxiong and Mamianshan basalts in the western Yangtze and northern Cathaysia blocks, respectively, have sub-chondritic Nb/Ta ratios (< 17.5), relative high Nb/La ratios and obvious crustal contamination trends, suggesting that they were derived mainly from OIB-like mantle sources with contamination of crustal materials. Data of the Suxiong and Mamianshan basalts are from from Li *et al.* (2002*a*) and Li, Li & Li (2005), respectively.

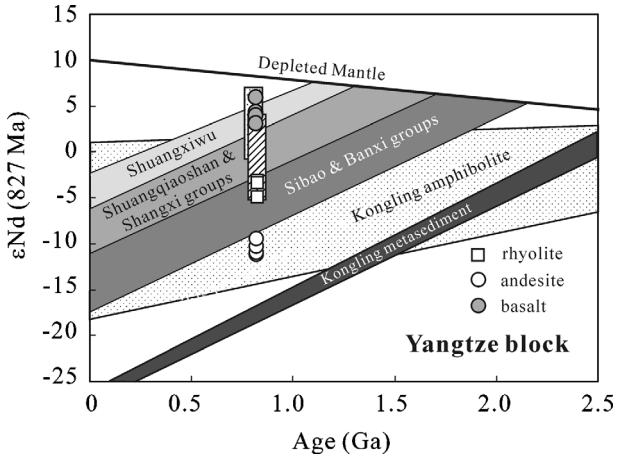

Figure 8. Nd isotopic evolution plot of the Guangfeng volcanic rocks. Nd isotopic evolution trends for the Yangtze Block are after Chen & Jahn, (1998) and Gao *et al.* (1999). Small vertical rectangles with dots and stripes indicate the Suxiong and Mamianshan basalts, respectively. Nd isotopic data from the Suxiong and Mamianshan basalts are from Li *et al.* (2002*a*) and Li, Li & Li (2005).

exclusively below 17.5 (Fig. 7a). Because the Nb/Ta ratios of lower to upper crust are in the range of 8.3 to 11.3 (Rudnick & Fountain, 1995), the super-chondritic Nb/Ta ratios of the Guangfeng basalts should have been inherited from the mantle source, rather than caused by the contamination of crustal material. Numerous experimental and geochemical studies indicate that siliceous melts derived from subducted oceanic slab have super-chondritic Nb/Ta ratios due to residual rutile in the source which could significantly fractionate Nb from Ta, whereas the opposite effect was observed for rutile in slab-derived fluids (Green & Pearson, 1987; Brenan *et al.* 1994; Keppler, 1996; Stolz *et al.* 1996; Münker, 1998; Münker *et al.* 2004; Xiong, Adam & Green, 2005; Xiong *et al.* 2006; Xiong, 2006). Therefore, the Guangfeng basaltic rocks were most likely generated by partial melting of a subcontinental lithospheric mantle source that had been metasomatized by slab-derived melts. Their T_{DM} ages of 1.0–1.2 Ga suggest that the mantle metasomatism might have taken place shortly before their formation, possibly during the *c.* 1.1–0.9 Ga Sibao orogeny (e.g. Li *et al.* 2002*b*, 2007*c*; Li & Li, 2003; Ye *et al.* 2007).

5.b. Andesitic rocks

Three main viewpoints have been proposed to interpret the origin of andesitic rocks: (1) fractionated crystallization of basaltic rocks derived from mantle peridotite; (2) dehydration partial melting of metabasalts (amphibolites) or metasedimentary rocks in the lower or middle crust by underplating and/or intrusions of hot, mantle-derived magma; and (3) mixing of mantle-derived basaltic magmas with crust-derived felsic melts.

The Guangfeng andesitic rocks have significantly lower εNd(T) values (between −9.3 and −11.1) than the associated basaltic rocks which have high positive εNd(T) values of 3.1 to 6.0, indicating that the andesitic rocks were unlikely to have originated by simple fractional crystallization of the basaltic parental magmas. The andesites are characterized by a wide range of SiO_2 contents (57.62–65.60 %) and early Palaeoproterozoic T_{2DM} ages of 2.3–2.4 Ga, suggesting significant involvement of ancient crustal components. Furthermore, their T_{2DM} values are obviously older than most pre-900 Ma metasedimentary rocks in the southeastern margin of the Yangtze Block (e.g. Chen & Jahn, 1998; Li & McCulloch, 1996), indicating that there likely exist unexposed ancient crustal rocks (Fig. 8). Such Palaeoproterozoic- to Archaean-aged basement rocks are exposed in the Kongling area of the northern Yangtze Block only (Gao *et al.* 1999; Qiu *et al.* 2000; Zhang *et al.* 2006*a*,*b*), but could be widespread

beneath the whole Yangtze Block as well (e.g. Zheng *et al.* 2006; Greentree *et al.* 2006). Although the Kongling amphibolites have εNd(T) values between 1.5 and −11.9 at 825 Ma, broadly consistent with the εNd(T) values of Guangfeng andesites (−9.3 to −11.1), equilibrium partial melting calculations on the basis of the trace elements (Nb and Zr) indicate that it would require about 60–70 % melting of the Kongling amphibolites to match the trace element features of the Guangfeng andesites (assuming the residual mineral assemblage is Pl:Cpx:Opx:Mt ≈ 55:30:5:10 and $D_{Nb} = 0.23$, $D_{Zr} = 0.11$: Beard & Lofgren, 1991; Rollinson, 1993). Such large degrees of melting are inconceivable and inconsistent with the experimental results (SiO_2 generally > 60 % and melting percentage < 40 % at water-unsaturated dehydration condition: Beard & Lofgren, 1991). Therefore, partial melting of the Archaean amphibolites alone is unlikely to have produced the Guangfeng andesite.

It is noteworthy that the εNd(T) values of the Guangfeng andesitic rocks are even lower than those of the associated felsic volcanic rocks (εNd(T) = −2.9 to −4.7), indicating that these andesitic rocks could not have been formed by mixing of mantle-derived basaltic magmas and associated felsic melts. However, generation by mixing of basaltic magmas with felsic melts derived from unexposed ancient middle-lower crustal rocks, such as the Kongling metasedimentary rocks (e.g. Gao *et al.* 1999), is possible. Two-component mixing calculations suggest that the Guangfeng andesites could have been formed by mixing of the associated basalts with about 30–40 % of the Kongling metasediments (Fig. 9a, b). It is noted that the andesitic rocks have a wide range of SiO_2 and their Th/Ta ratios increase slightly with increasing Zr content (Fig. 9c), suggesting strong fractional crystallization. Niobium, Th and REE are positively correlated with Zr (Fig. 3), suggesting that clinopyroxene and plagioclase are predominant minerals involved in fractional crystallization, because the partition coefficients of these elements in clinopyroxene and plagioclase are < 1 for the andesitic melts, whereas they are > 1 in amphibole (Rollinson, 1993).

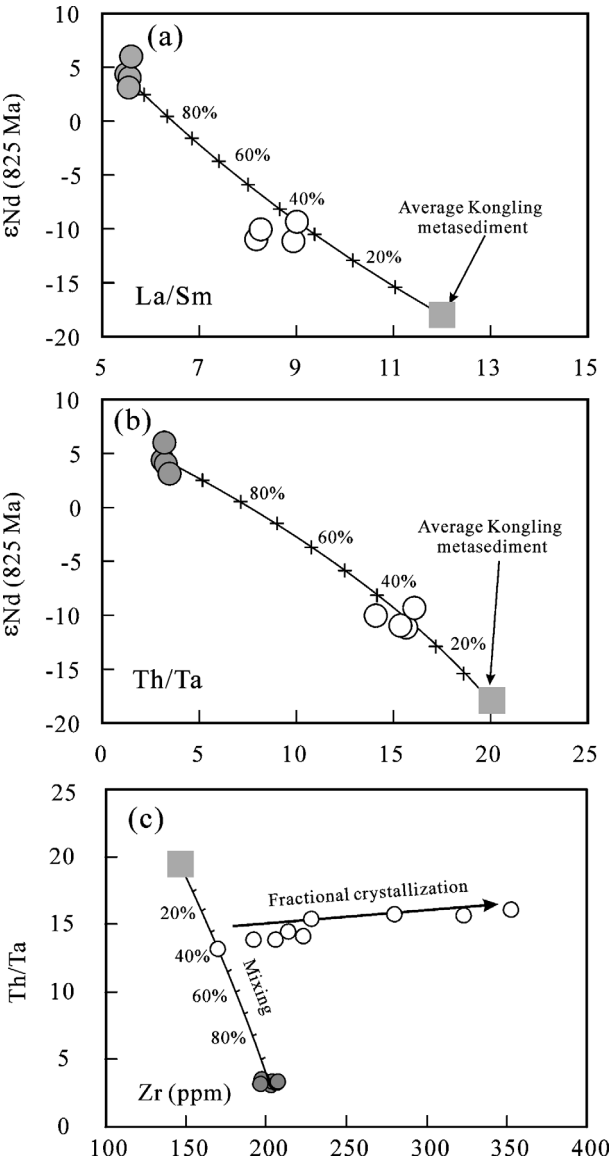

Figure 9. Plots of (a) εNd(T) v. La/Sm, (b) εNd(T) v. Th/Ta and (c) Th/Ta v. Zr, showing two-component mixing modal calculation for the generation of the Guangfeng andesites. The andesites could have been formed by mixing of evolved basalt magmas with about 30–40 % felsic melts derived from the Archaean Kongling metasediments (Gao *et al.* 1999), followed by fractional crystallization. Symbols are as in Figure 3.

5.c. Felsic rocks

The Guangfeng rhyolites are peraluminous with A/CNK values of > 1.6. They have relatively homogeneous negative εNd(T) values of −2.9 to −4.7 and late Palaeoproterozoic T_{2DM} ages of 1.7–1.9 Ga. Overall, their geochemical features are similar to those of the *c.* 820 Ma peraluminous granitoids in the southern Anhui and northeastern Jiangxi provinces (Li *et al.* 2003*a*; Wu *et al.* 2006), suggesting a predominant contribution from late Palaeoproterozoic to Mesoproterozoic crustal source (Fig. 8). These rocks are high in Zr (148–218 ppm), corresponding to the zircon saturation temperatures (T_{Zr}) of between 817 and 862 °C (Table 2). In combination with their relatively low Al_2O_3/TiO_2 ratios of < 70, the rhyolite rocks were likely generated by high temperature partial melting (Sylvester, 1998) of metasedimentary rocks caused by hot mantle upwelling, or basaltic magma underplating and/or intrusions during lithospheric thinning in a continental rift environment.

6. Tectonic significance

SHRIMP U–Pb zircon dating results indicate that the Guangfeng volcanic rocks were formed at *c.* 825 Ma. They are coeval with the widespread Neoproterozoic

syn-rift basaltic and felsic volcanic rocks throughout South China, including the 817 ± 5 Ma Tiechuanshan bimodal basalte–dacite/rhyolite in the northwestern Yangtze Block (Ling *et al.* 2003), the 800–810 Ma Suxiong bimodal basalt–dacite/rhyolite along the western margin of the Yangtze Block (Li *et al.* 2002*a*), the 819 ± 11 Ma Yingyangguan spilite–keratophyre (Zhou *et al.* 2002*a*), the 814 ± 12 Ma Changshuipu dacitic agglomerate (Wang *et al.* 2003) in southern Yangtze Block, and the 818 ± 9 Ma Mamianshan bimodal volcanic rocks in northern Cathaysia (Li, Li & Li, 2005). This giant magmatic event was commonly considered to be a result of anorogenic magmatism caused by the *c.* 825 Ma South China mantle plume that triggered the initial rifting of the supercontinent Rodinia (Li, 1999; Li *et al.* 2002*a*, 2003*a*; Wang *et al.* 2007). Moreover, compared with similar-aged anorogenic magmatism recorded in numerous other Rodinian continents, Li *et al.* (2003*b*) proposed that a mantle superplume caused the global-scale contemporaneous magmatism at *c.* 830–740 Ma. In contrast, some other workers speculated that active continental margins existed around the Yangtze Block during middle Neoproterozoic times, and the 860–750 Ma igneous rocks are products related to subduction of oceanic plate and collision between the Yangtze and Cathaysia blocks (e.g. Zhou *et al.* 2002*b*,*c*, 2006*a*,*b*; Wang *et al.* 2004, 2006; Munteanu & Yao, 2007). This arc model is mainly based on some 'arc-like' geochemical signatures such as depletion of Nb and Ta relative to La and Th, but inconsistent with many aspects of geological observations (e.g. Li *et al.* 2007*a*,*b*).

We emphasize that Nb–Ta depletion in some middle Neoproterozoic basalts in South China is mainly attributed to either derivation from the metasomatized mantle sources or contamination by crustal components. Figure 7a and b are plots of Nb/Ta and εNd(T) v. Nb/La for three similar-aged (*c.* 820–800 Ma) alkaline basalts from Suxiong of the western Yangzte Block, Mamianshan of northern Cathaysia and Guangfeng of this study (also see Fig. 1a). Both the Suxiong and Mamianshan basalts display obvious trends between the OIB-type mantle-derived magmas and the crustal components, whereas the Guangfeng basalts are derived dominantly from a metasomatized mantle source. It has been argued that the Suxiong and Mamianshan alkaline basalts are typical products of intracontinental rifting magmatism. Despite showing varying degrees of depletion in Nb and Ta relative to La and Th, the Guangfeng basalts also show a broad geochemical similarity to typical intraplate basalts, similar to other middle Neoproterozoic basalts and dykes in South China that also show Nb and Ta depletions (e.g. Li *et al.* 2003*a*; Ling *et al.* 2003; Lin, Li & Li 2007; Zhou *et al.* 2007). Intraplate magmatic rocks with Nb and Ta depletion are also seen in other continents (e.g. Harry & Leeman, 1995; Hawkesworth *et al.* 1995; Morris, Larson & Hooper, 2000; Romer, Forster & Breitkreuz, 2001), which are mostly associated with former plate convergence zones. Therefore, depletion of Nb and Ta in basaltic rocks cannot be simplistically used as a definitive indicator for active subduction tectonic settings.

7. Conclusions

SHRIMP U–Pb zircon analysis suggests that the Guangfeng volcanic rocks were erupted at 827 ± 14 Ma, coeval with the early phase of middle Neoproterzoic rift-related igneous rocks in South China and other Rodinia continents. They were generated by partial melting of a slab melt-metasomatized subcontinental lithospheric mantle source in an intracontinental rifting setting. The associated andesites were likely generated by mixing of fractionated basaltic melts with felsic melts derived from the Archaean metasedimentary rocks, followed by fractional crystallization of clinopyroxene and plagioclase. The rhyolites were derived from Mesoproterozoic sedimentary sources at relatively shallow levels. We thus concluded that the Guangfeng volcanic suite is a magmatic response of different levels of continental lithosphere (including lithospheric mantle and the lower–middle to upper crustal levels) to the middle Neoproterozoic intracontinental rifting possibly caused by a mantle plume. These syn-rifting volcanic rocks inherited some 'arc-like' geochemical signatures from their sources, consistent with the fact that the Guangfeng rift basin was developed within a former mobile zone.

Acknowledgements. We appreciate the assistance of Y. Liu, X. L. Tu, and X. R. Liang in geochemical and Nd isotopic analyses, and B. Song and H. Tao in SHRIMP U–Pb zircon analyses, J. Wang and C.M. Bao are thanked for help with field work; X.C. Wang is thanked for help with modal calculation. Review comments of Drs M. Sun, Y. F. Zheng and X. L. Wang have been helpful. We particularly thank the editor Dr David Pyle for his detailed and constructive review on an early version of this paper. This work was supported by the Chinese Academy of Sciences (KZCX3-SW-141, 2003-1-2) and NSFC (grants 40421303, 40372040 and 40573016) and ARC Discovery Project grants (DP0450020 and DP0770228). This is TIGeR (The Institute of Geoscience Research) publication no. 69.

References

BEARD, J. S. & LOFGREN, G. E. 1991. Dehydration melting and water saturated melting of basaltic and andesitic greenstones and amphibolites at 1, 3 and 6.9 kb. *Journal of Petrology* **32**, 365–401.

BLACK, L. P., KAMO, S. L., ALLEN, C. M., ALEINIKOFF, J. N., DAVIS, D. W., KORSCH, R. J. & FOUDOULIS, C. 2003. TEMORA 1: a new zircon standard for Phanerozoic U–Pb geochronology. *Chemical Geology* **200**, 155–70.

BRENAN, J. M., SHAW, H. F., PHINNEY, D. L. & RYERSON, F. J. 1994. Rutile–aqueous fluid partitioning of Nb,

Ta, Hf, Zr, U and Th: implications for high field strength element depletions in islandarc basalts. *Earth and Planetary Science Letters* **128**, 327–39.

CHEN, J. F. & JAHN, B. M. 1998. Crustal evolution of southeastern China: Nd and Sr isotopic evidence. *Tectonophysics* **284**, 101–33.

CUMMING, G. L. & RICHARDS, J. R. 1975. Ore lead isotope ratios in a continuously changing earth. *Earth and Planetary Science Letters* **28**, 155–71.

GAO, S., LING, W. L., QIU, Y. M., ZHOU, L., HARTMANN, G. & SIMON, K. 1999. Contrasting geochemical and Sm–Nd isotopic compositions of Archean metasediments from the Kongling high-grade terrain of the Yangtze Craton: Evidence for cratonic evolution and redistribution of REE during crustal anatexia. *Geochimica et Cosmochimica Acta* **63**, 2071–88.

GIBSON, S. A., KIRKPATRICK, R. J., EMMERMAN, R., SCHMINCKE, P.-H., PRITCHARD, G., OKAY, P. J., THORPE, R. S. & MARRINER, G. F. 1982. The trace element composition of the lavas and dykes from a 3 km vertical section through a lava pile of Eastern Iceland. *Journal of Geophysical Research* **87**, 6532–46.

GREEN, T. H. & PEARSON, N. J. 1987. An experimental study of Nb and Ta partitioning between Ti-rich minerals and silicate liquids at high pressure and temperature. *Geochimica et Cosmochimica Acta* **51**, 55–62.

GREENTREE, M. R., LI, Z. X., LI, X. H. & WU, H. 2006. Late Mesoproterozoic to earliest Neoproterozoic basin record of the Sibao orogenesis in western South China and relationship to the assembly of Rodinia. *Precambrian Research* **151**, 79–100.

GUAN, T. & YU, D. 1993. Characteristics and geological significance on the strata section of earlier late Proterozoic era in Guangfeng area of Jiangxi. *Journal of East China Geological Institute* **16**(4), 385–94 (in Chinese with English abstract).

HARRY, D. L. & LEEMAN, W. P. 1995. Partial melting of melt metasomatized subcontinental mantle and magma source potential of the lower lithosphere. *Journal of Geophysical Research* **100**, 10255–69.

HAWKESWORTH, C., TURNER, S., GALLAGHER, K., HUNTER, A., BRADSHAW, T. & ROGERS, N. 1995. Calc-alkaline magmatism, lithospheric thinning and extension in the Basin and Range. *Journal of Geophysical Research* **100**, 10271–86.

KEPPLER, H. 1996. Constraints from partitioning experiments on the composition of subduction-zone fluids. *Nature* **380**, 237–40.

LI, W. X. & LI, X. H. 2003. Adakitic granites within the NE Jiangxi ophiolites, South China: geochemical and Nd isotopic evidence. *Precambrian Research* **122**, 29–44.

LI, W. X., LI, X. H. & LI, Z. X. 2005. Neoproterozoic bimodal magmatism in the Cathaysia Block of South China and its tectonic significance. *Precambrian Research* **136**, 51–66.

LI, X. H. 1997. Timing of the Cathaysia block formation: constraints from SHRIMP U–Pb zircon geochronology. *Episodes* **20**, 188–92.

LI, X. H. 1999. U–Pb zircon ages of granites from the southern margin of the Yangtze block: Timing of the Neoproterozoic Jinning orogeny in SE China and implications for Rodinia. *Precambrian Research* **97**, 43–57.

LI, X. H., LI, Z. X., GE, W., ZHOU, H., LI, W. X., LIU, Y. & WINGATE, M. T. D. 2003*a*. Neoproterozoic granitoids in South China: crustal melting above a mantle plume at 825 Ma? *Precambrian Research* **122**, 45–83.

LI, X. H., LI, Z. X., SINCLAIR, J. A., LI, W. X. & CARTER, G. 2006. Revisiting the "Yanbian Terrane": Implications for Neoproterozoic tectonic evolution of the western Yangtze Block, South China. *Precambrian Research* **151**, 14–30.

LI, X. H., LI, Z. X., SINCLAIR, J. A., LI, W. X. & CARTER, G. 2007*a*. Reply to the comment by Zhou *et al.* on: "Revisiting the 'Yanbian Terrane': Implications for Neoproterozoic tectonic evolution of the western Yangtze Block, South China". *Precambrian Research* **155**, 318–23.

LI, X. H., LI, Z. X., SINCLAIR, J. A., LI, W. X. & CARTER, G. 2007*b*. Understanding dual geochemical characters in a geological context for the Gaojiacun intrusion: Response to Munteanu and Yao's discussion. *Precambrian Research* **155**, 328–32.

LI, X. H., LI, Z. X., ZHOU, H., LIU, Y. & KINNY, P. D. 2002*a*. U–Pb zircon geochronology, geochemistry and Nd isotopic study of Neoproterozoic bimodal volcanic rocks in the Kangdian Rift of South China: implications for the initial rifting of Rodinia. *Precambrian Research* **113**, 135–54.

LI, X. H., LIU, D. Y., SUN, M., LI, W. X., LIANG, X. R. & LIU, Y. 2004. Precise Sm–Nd and U–Pb isotopic dating of the super-giant Shizhuyuan polymetallic deposit and its host granite, Southeast China. *Geological Magazine* **141**, 225–31.

LI, X. H. & MCCULLOCH, M. T. 1996. Secular variation in the Nd isotopic composition of Neoproterozoic sediments from the southern margin of the Yangtze Block: evidence for a Proterozoic continental collision in southeast China. *Precambrian Research* **76**, 67–76.

LI, X. H., QI, C. S., LIU, Y., LIANG, X. R., TU, X. L., XIE, L. W. & YANG, Y. H. 2005. Petrogenesis of the Neoproterozoic bimodal volcanic rocks along the western margin of the Yangtze Block: new constraints from Hf isotopes and Fe/Mn ratios. *Chinese Science Bulletin* **50**, 2481–6.

LI, X. H., SUN, M., WEI, G. J., LIU, Y., LEE, C. Y. & MALPAS, J. G. 2000. Geochemical and Sm–Nd isotopic study of amphibolites in the Cathaysia block, SE China: evidence for extremely depleted mantle in the Paleoproterozoic. *Precambrian Research* **102**, 251–62.

LI, Z. X. & LI, X. H. 2007. Formation of the 1300 km-wide intra-continental orogen and post-orogenic magmatic province in Mesozoic South China: A flat-slab subduction model. *Geology* **35**, 179–82.

LI, Z. X., LI, X. H., KINNY, P. D. & WANG, J. 1999. The breakup of Rodinia: did it start with a mantle plume beneath South China? *Earth and Planetary Science Letters* **173**, 171–81.

LI, Z. X., LI, X. H., KINNY, P. D., WANG, J., ZHANG, S. & ZHOU, H. 2003*b*. Geochronology of Neoproterozoic syn-rift magmatism in the Yangtze Craton, South China and correlations with other continents: evidence for a mantle superplume that broke up Rodinia. *Precambrian Research* **122**, 85–109.

LI, Z. X., LI, X. H., ZHOU, H. & KINNY, P. D. 2002*b*. Grenville-aged continental collision in South China: new SHRIMP U–Pb zircon results and implications for Rodinia configuration. *Geology* **30**, 163–6.

LI, Z. X., WANG, J., LI, X. H. & ZHANG, S. H. 2003*c*. *From Sibao orogenesis to Nanhua rifting: late Precambrian tectonic history of eastern South China – an overview and field guide*. Beijing: Geological Publishing House, 100 pp.

LI, Z. X., WARTHO, J. A., OCCHIPINTI, S., ZHANG, C. L., LI, X. H., WANG, J. & BAO, C. 2007*c*. Early history of the eastern Sibao Orogen (South China) during the assembly of Rodinia: new mica $^{40}Ar/^{39}Ar$ dating and SHRIMP U–Pb detrital zircon provenance constraints. *Precambrian Research* **159**, 79–94.

LIN, G. C., LI, X. H. & LI, W. X. 2007. SHRIMP U–Pb zircon age, geochemistry and Nd–Hf isotope of Neoproterozoic mafic dyke swarms in western Sichuan: Petrogenesis and tectonic significance. *Science in China Series D* **50**, 1–16.

LING, W., GAO, S., ZHANG, B., LI, H., LIU, Y. & CHENG, J. 2003. Neoproterozoic tectonic evolution of the northwestern Yangtze Craton, South China: implications for amalgamation and break-up of the Rodinia Supercontinent. *Precambrian Research* **122**, 111–40.

MCCULLOCH, M. T. & GAMBLE, J. A. 1991. Geochemical and geodynamical conatraints on subduction zone magmatism. *Earth and Planetary Science Letters* **102**, 358–74.

MILLER, C. F., MCDOWELL, S. M. & MAPES, R. W. 2003. Hot and cold granites? Implications of zircon saturation temperatures and preservation of inheritance. *Geology* **31**, 529–32.

MORRIS, G. A., LARSON, P. B. & HOOPER, P. R. 2000. "Subduction style" magmatism in a non-subduction setting: the Colville Igneous Complex, NE Washington State, USA. *Journal of Petrology* **41**, 43–67.

MÜNKER, C. 1998. Nb/Ta fractionation in a Cambrian arc/back arc system, New Zealand: source constraints and application of refined ICPMS techniques. *Chemical Geology* **144**, 23–45.

MÜNKER, C., WÖRNER, G., YOGODZINSKI, G. & CHURIKOVA, T. 2004. Behaviour of high field strength elements in subduction zones: constraints from Kamchatka–Aleutian arc lavas. *Earth and Planetary Science Letters* **224**, 275–93.

MUNTEANU, M. & YAO, Y. 2007. The Gaojiacun intrusion: Rift- or subduction-related?: Comment on "Revisiting the 'Yanbian Terrane': Implications for Neoproterozoic tectonic evolution of the western Yangtze Block, South China" by Li et al. (2006). *Precambrian Research* **155**, 324–7.

NELSON, D. R. 1997. *Compilation of SHRIMP U–Pb zircon geochronology data, 1996*. Geological Survey of Western Australia Record 1997/2. Perth: Geological Survey of Western Australia, 189 pp.

PEARCE, J. A. & CANN, J. R. 1973. Tectonic setting of basaltic volcanic rocks determined using trace element analyses. *Earth and Planetary Science Letters* **19**, 290–300.

QIU, Y. M., GAO, S., MCNAUGHTON, N. J., GROVES, D. I. & LING, W. L. 2000. First evidence of >3.2 Ga continental crust in the Yangtze Craton of south China and its implications for Archean crustal evolution and Phanerozoic tectonics. *Geology* **28**, 11–14.

ROLLINSON, H. 1993. *Using geochemical data: evaluation, presentation, interpretation*. Singapore: John Wiley & Sons Inc., 352 pp.

ROMER, R. L., FORSTER, H.-J. & BREITKREUZ, C. 2001. Intracontinental extensional magmatism with a subduction fingerprint: the late Carboniferous Halle Volcanic Complex (Germany). *Contributions to Mineralogy and Petrology* **141**, 201–21.

RUDNICK, R. L. & FOUNTAIN, D. M. 1995. Nature and composition of the continental crust: a lower crustal perspective. *Reviews of Geophysics* **33**, 267–309.

STOLZ, A. J., JOCHUM, K. P., SPETTEL, B. & HOFMANN, A. W. 1996. Fluid- and melt-related enrichment in the subarc mantle: evidence from Nb/Ta variations in island-arc basalt. *Geology* **24**, 587–90.

SUN, S.-S. & MCDONOUGH, W. F. 1989. Chemical and isotopic systematics of oceanic basalts: implications for mantle composition and processes. In *Magmatism in the Ocean Basins* (eds A. D. Saunders & M. J. Norry), pp. 313–45. Geological Society of London, Special Publication no. 42.

SYLVESTER, P. J. 1998. Post-collisional strongly peraluminous granites. *Lithos* **45**, 29–44.

TANAKA, T. and 19 co-authors. 2000. JNdi-1: a neodymium isotopic reference in consistency with LaJolla neodymium. *Chemical Geology* **168**, 279–81.

VERMEESCH, P. 2006. Tectonic discrimination of basalts with classification trees. *Geochimica et Cosmochimica Acta* **70**, 1839–48.

WANG, J. & GAO, Y. 2003. Sedimentary evolution of the Guangfeng Neoproterozoic rift sub-basin, northeastern Jiangxi, South China. *IGCP 440 South China Field Symposium Abstract*, pp. 52–4.

WANG, J., LI, X. H., DUAN, T. Z., LIU, D. Y., SONG, B., LI, Z. & GAO, Y. 2003. Zircon SHRIMP U–Pb dating for the Cangshuipu volcanic rocks and its implications for the lower boundary age of the Nanhua strata in South China. *Chinese Science Bulletin* **48**, 1663–9.

WANG, J. & LI, Z. X. 2003. History of Neoproterozoic rift basins in South China: implications for Rodinia breakup. *Precambrian Research* **122**, 141–58.

WANG, X. C., LI, X. H., LI, W. X. & LI, Z. X. 2007. Ca. 825 Ma komatiitic basalts in South China: First evidence for >1500 °C mantle melts by a Rodinian mantle plume. *Geology* **35**, 1103–6.

WANG, X. L., ZHOU, J. C., QIU, J. S. & GAO, J. F. 2004. Geochemistry of the Meso- to Neoproterozoic basic–acid rocks from Hunan Province, South China: implications for the evolution of the western Jiangnan orogen. *Precambrian Research* **135**, 79–103.

WANG, X. L., ZHOU, J. C., QIU, J. S., ZHANG, W. L., LIU, X. M. & ZHANG, G. L. 2006. LA-ICP-MS U–Pb zircon geochronology of the Neoproterozoic igneous rocks from Northern Guangxi, South China: implications for tectonic evolution. *Precambrian Research* **145**, 111–30.

WATSON, E. B. & HARRISON, T. M. 1983. Zircon saturation revisited: temperature and composition effects in a variety of crustal magma types. *Earth and Planetary Science Letters* **64**, 295–304.

WILLIAMS, I. S. 1998. U–Th–Pb geochronology by ion microprobe. Applications of Microanalytical Techniques to Understanding Mineralizing Processes. *Review of Economic Geology* **7**, 1–35.

WINGATE, M. T. D., CAMPBELL, I. H., COMPSTON, W. & GIBSON, G. M. 1998. Ion microprobe U–Pb ages for Neoproterozoic basaltic magmatism in south-central Australia and implications for the breakup of Rodinia. *Precambrian Research* **87**, 135–59.

WU, R. X., ZHENG, Y. F., WU, Y. B., ZHAO, Z. F., ZHANG, S. B., LIU, X. M. & WU, F. Y. 2006. Reworking of juvenile crust: Element and isotope evidence from Neoproterozoic granodiorite in South China. *Precambrian Research* **146**, 179–212.

XIONG, X. L., ADAM, J. & GREEN, T. H. 2005. Rutile stability and rutile/melt HFSE partitioning during partial melting of hydrous basalt: implications for TTG genesis. *Chemical Geology* **218**, 339–59.

XIONG, X. L. 2006. Trace element evidence for growth of earth continental crust by melting of rutile-bearing hydrous eclogite. *Geology* **34**, 945–8.

XIONG, X. L., XIA, B., XU, J. F., NIU, H. C. & XIAO, W. S. 2006. Na depletion in modern adakites via melt/rock reaction within the sub-arc mantle. *Chemical Geology* **229**, 273–92.

YE, M. F., LI, X. H., LI, W. X., LIU, Y. & LI, Z. X. 2007. SHRIMP zircon U–Pb geochronological and whole-rock geochemical evidence for an early Neoproterozoic Sibaoan magmatic arc along the southeastern margin of the Yangtze Block. *Gondwana Research* **12**, 144–56.

ZHANG, L. M., YAN, Y. K. & YAN, Y. Z. 1991. Microplant species of Guangfeng Group in the NE Jiangxi province: Discovery and significance. *Journal of Stratigraphy* **15**, 263–9 (in Chinese with English abstract).

ZHANG, S. B., ZHENG, Y. F., WU, Y. B., ZHAO, Z. F., GAO, S. & WU, F. Y. 2006*a*. Zircon isotope evidence for ≥3.5 Ga continental crust in the Yangtze craton of China. *Precambrian Research* **146**, 16–34.

ZHANG, S. B., ZHENG, Y. F., WU, Y. B., ZHAO, Z. F., GAO, S., WU, F. Y., 2006*b*. Zircon U–Pb age and Hf–O isotope evidence for Paleoproterozoic metamorphic event in South China. *Precambrian Research* **151**, 265–88.

ZHAO, J. X., MALCOLM, M. T. & KORSCH, R. J. 1994. Characterisation of a plume-related ~800 Ma magmatic event and its implications for basin formation in central-southern Australia. *Earth and Planetary Science Letters* **121**, 349–67.

ZHENG, J., GRIFFIN, W. L., O'REILLY, S. Y., ZHENG, M., PEARSON, N. & PAN, Y. 2006. Widespread Archean basement beneath the Yangtze craton. *Geology* **34**, 417–20.

ZHOU, C. M., TUCKER, R., XIAO, S., PENG, Z., YUAN, X. & CHEN, Z. 2004. New constraints on the ages of Neoproterozoic glaciations in south China. *Geology* **32**, 437–40.

ZHOU, H., LI, X. H., WANG, H., LI, J. & LI, H. 2002*as*. U–Pb zircon geochronology of basic volcanic rocks within the Yingyangguan Group in Hezhou, Guangxi, and its tectonic implications. *Geology Review* **48** (Suppl.), 22–5 (in Chinese with English abstract).

ZHOU, M. F., KENNEDY, A. K., SUN, M., MALPAS, J. & LESHER, C. M. 2002*b*. Neoproterozoic arc-related mafic intrusions along the northern margin of South China: implications for the accretion of Rodinia. *Journal of Geology* **110**, 611–18.

ZHOU, M. F., YAN, D. P., KENNEDY, A. K., LI, Y. & DING, J. 2002*c*. SHRIMP U–Pb zircon geochronological and geochemical evidence for Neoproterozoic arc-magmatism along the western margin of the Yangtze Block, South China. *Earth and Planetary Science Letters* **196**, 51–67.

ZHOU, M. F., MA, Y., YAN, D. P., XIA, X., ZHAO, J. H. & SUN, M. 2006*a*. The Yanbian Terrane (Southern Sichuan Province, SW China): A Neoproterozoic arc assemblage in the western margin of the Yangtze Block. *Precambrian Research* **144**, 19–38.

ZHOU, M. F., YAN, D. P., WANG, C. L., XIA, X., ZHAO, J. H. & SUN, M. 2006*b*. Subduction-related origin of the 750 Ma Xuelongbao adakitic complex (Sichuan Province, China): implications for the tectonic setting of the giant Neoproterozoic magmatic event in South China. *Earth and Planetary Science Letters* **248**, 271–85.

ZHOU, J. B., LI, X. H., GE, W. C. & LI, Z. X. 2007. Age and origin of Middle Neoproterozoic mafic magmatism in southern Yangtze Block and relevance to the break-up of Rodinia. *Gondwana Research* **12**, 184–97.